Int. J. Heat Mass Transfer. Vol. 13, pp. 1479–1496. Pergamon Press 1970. Printed in Great Britain

THERMOCONVECTIVE INSTABILITY IN A BOUNDED CYLINDRICAL FLUID LAYER

G. S. CHARLSON and R. L. SANI

Department of Chemistry and Chemical Engineering, University of Illinois, Urbana, Illinois, U.S.A.

(*Received* 29 *September* 1969 *and in revised form* 13 *January* 1970)

Abstract—The onset of axisymmetric convection in cylindrical layers of fluid heated from beneath is investigated for various radius-to-height ratios. Upper as well as lower bounds on the critical Rayleigh number for such flows are computed, and the structure of the convective flow is investigated. The latter is in good agreement with the observation of Koschmieder.

NOMENCLATURE

A, characteristic amplitude of flow;
A_{ij}, coefficients in temperative field representation (23);
a, wave number;
B_{ij}, coefficients in velocity field representation (22);
C_p, specific heat at constant pressure;
da, boundary surface element;
dv, volume element;
$\mathbf{e}_r\mathbf{e}_\varphi, \mathbf{e}_z$, unit vectors;
g, acceleration of gravity;
I, bilinear functional (32);
$J_0(r)$, zeroth order Bessel function of the first kind;
$J_1(r)$; first order Bessel function of the first kind;
k, thermal conductivity;
$\mathbf{L}$, linear operator;
L, height of cylinder;
M, number of r-trial functions;
N, number of z-trial functions;
$\mathbf{n}$, unit outward pointing normal on V;
$\bar{P}$, pressure field;
P, dimensionless pressure field, $L^2\bar{P}/\rho_0\nu\kappa Ra^{\frac{1}{2}}$;
p, spatial part of pressure field representation (12);
Pr, Prandtl number $\equiv \nu/\kappa$;
R, radius of cylinder;
$\bar{r}$, radial coordinate;
r, dimensionless radial coordinate, $\bar{r}/\gamma L$;
Ra, Rayleigh number $\equiv \alpha(T_0 - T_1)gL^3/\nu\kappa$;
Ra_i, ith Rayleigh number;
T, temperature field;
$\bar{t}$, time;
t, dimensionless time, $\kappa\bar{t}/L^2$;
$\bar{\mathbf{U}}$, velocity field $\equiv (\bar{U}_r, \bar{U}_\varphi, \bar{U}_z)$;
$\mathbf{U}$, dimensionless velocity field, $\bar{\mathbf{U}}L/\kappa Ra^{\frac{1}{2}}$;
$\mathbf{u}$, spatial part of velocity field representation (10);
V, cylindrical domain;
w, vertical component of dimensionless velocity;
X, z-trial function;
Y, r-trial function;
$\bar{z}$, vertical coordinate;
z, dimensionless vertical coordinate, $\bar{z}/L$.

Greek symbols

α, thermal coefficient of expansion at T_0;
α_k, roots of (30) or (31);
γ, aspect ratio $\equiv R/L$;
δ^4, eigenvalue in (28);
ϵ, "contained in";

η, roots of $J_1(a\gamma)$;
$\overline{\Theta}$, perturbation in temperature field;
Θ, dimensionless perturbation in temperature field, $\overline{\Theta}/(T_0 - T_1)$;
θ, spatial part of temperature field representation (11);
κ, thermal diffusivity $\equiv k/C_p\rho_0$;
λ, inverse of square root of Rayleigh number $\equiv Ra^{-\frac{1}{2}}$;
μ, viscosity;
ν, kinematic viscosity $\equiv \mu/\rho_0$;
ξ^4, eigenvalue in (25);
ρ, density;
σ, growth rate factor;
φ, azimuthal coordinate;
ψ, Stokes stream function.

Special symbols
∂V, boundary of the cylindrical domain V;
$\mathscr{V}$, linear vector space.

Superscripts
†, transpose;
$'$, derivative with respect to r or z, or used in designating linear vector spaces;
*, adjoint;
$\tilde{}$, complex conjugate.

Subscripts
1, upper boundary;
0, lower boundary;
r, real part;
i, imaginary part or summation index.

1. INTRODUCTION

THE INVESTIGATION of the buoyancy driven instability of a quiescent fluid layer, heated from below in the presence of a gravitational field, was motivated initially by the experiments of Bénard on thin fluid layers [1, 2], although it was later shown that he observed surface tension driven instability [3, 4]. In order to account for the experimental observations of Bénard, Lord Rayleigh performed an analysis [5] based on the assumption that the instability was buoyancy driven. His linearized theory provided the initial stimulus to the area of hydrodynamic stability. Since that time, the linear stability theory of a fluid layer of infinite extent has been refined considerably (see Chandrasekhar [6]), and nonlinear stability analyses have been applied, particularly with regard to the prediction of the preferred shape of the convective cells at the onset of convection. In contrast, a relatively small number of theoretical analyses appropriate to systems of bounded lateral extent are available in the literature. (Some examples include Ostrach and Pneuli [7], Zierep [8], Davis [9, 10], Liang *et al.* [11] and Edwards [12].

Recent elaborate experimental studies aimed at verifying the theoretical predictions of infinite layer analyses have not lead to consistent observations. For example, Koschmieder [13], in approximating an infinite layer by a thin fluid layer confined between rectangular or cylindrical walls, observed only stable rolls of geometric shape similar to that of the confining vessel. On the other hand, Chen and Whitehead [14] observed stable rolls and essentially straight boundaries in the cylindrical geometry. As pointed out by Newell and Whitehead [15] and Segel [16], the sidewall effect dominated the pattern of flow in Koschmieder's slow and carefully controlled experiments whereas this was not the case in the experiments of Chen and Whitehead (see Segel [16] for a classification of the various type patterns). As conjectured by Segel [16], sidewall effects can be expected to dominate the observed pattern of flow for at least a certain range of aspect ratio (half-width to depth ratio) if a characteristic measure of the vertical asymmetry induced in the dynamic state by, for example, variation of fluid properties with temperature [17], uniform heat generation [18], or the deflection of a free surface [19], is not too large. The present investigation focuses on one such "wall mode" of flow—the concentric circular rolls observed by Koschmieder.

There are two notable theoretical investigations of the effect of lateral walls, the first by Davis [9] and the second by Segel [16]. Davis [9], in a linear stability analysis of convection in a box, found that by considering the effect of lateral boundaries, results were obtained which agreed well with Koschmieder's observations for that particular geometry. Segel [16], using a multiple-scale perturbation analysis to modify the existing nonlinear results for infinite layers to approximate a "large" rectangular layer, obtained results similar to those of Davis [9] and clearly demonstrated the perturbing effect of the lateral boundaries.

Previous investigations of convective motion in a right circular cylinder have been performed by Pellew and Southwell [20], Zierep [8], Ostrach and Pneuli [7], and Liang *et al.* [11]. Pellew and Southwell, and Zierep noted that the presence of vertical walls prevented separation of variables in the usual fashion (see, for example, Chandrasekhar [6]), and consequently, only considered the idealized case of "slip" walls, which permitted separation of variables. Ostrach and Pneuli utilized the sixth order linear partial differential equation for the vertical component of velocity (w) after Jeffreys and others, and completed the description of the bounded system by specifying that $w = 0$, $\partial w/\partial z = 0$, and $\nabla_2^4 w = 0$ on the boundary of the container. However, on the vertical boundaries the condition $\partial w/\partial z = 0$, representing the tangential derivative of w, is merely a restatement of $w = 0$, and does not insure that the horizontal component of velocity vanishes on the vertical walls. Therefore, their results, obtained by separation of variables, do not describe the physical case of rigid side walls, except possibly for the case of a porous wall system with a certain amount of suction, or blowing, at the vertical boundaries. (It can be established by the method used in Section 5 that their method generates lower bounds to the critical Rayleigh number.) Subsequently, Sherman and Ostrach [21] utilized a valid formulation and generated a lower bound to the critical Rayleigh number. Liang *et al.* used a finite difference technique to investigate finite amplitude axisymmetric flow of a fluid with temperature dependent viscosity in a cylindrical geometry using a variety of boundary conditions. The aspect ratios (ratio of the radius to the height of the fluid layer) considered corresponded to cases in which a single roll filled the cylinder. At supercritical Rayleigh numbers, steady solutions were found with either upflow or downflow along the centerline of the cylinder depending on the initial state of the system. They also performed a perturbation analysis for insulated "slip" walls and free top and bottom surfaces. They found that the theory with temperature dependent viscosity predicted that only one of the steady solutions was stable near the critical. At sufficiently large Rayleigh numbers, two stable solutions were again predicted.

Because of the complexities involved in treating the general case of three-dimensional flow in a right circular cylinder, this work is limited to the mathematically simpler but physically realizable case of axisymmetric flow in a cylinder with a rigid top and bottom. The interest in such a flow stems from Koschmieder [13, 22, 23] who observed axisymmetric flows in both resting and rotating closed cylinders heated uniformly from below. Also, Soberman [24], in an earlier but not as carefully controlled experiment, observed axisymmetric flow for the case of a free top at an aspect ratio of 2·8.

The equations describing the dynamics of an infinitesimal disturbance introduced into an initially quiescent layer of fluid heated uniformly from below are analyzed for the case of axisymmetric flow by recasting them in a variational formulation and using the Rayleigh–Ritz method to approximate the solution. The streamlines calculated from the approximate solution are used to determine the number and size of the convective rolls. Calculations are performed for a range of aspect ratios from 0·5 to 8·0. Also, calculations at aspect ratios of 9·852, 10·30 and 12·987 are included for direct comparison to the experimental observations of Koschmieder.

2. MATHEMATICAL DESCRIPTION

The system under study consists of an initially motionless, boundary cylindrical layer of fluid uniformly heated from below. It is convenient to describe the system in terms of the cylindrical coordinate system shown in Fig. 1, such that

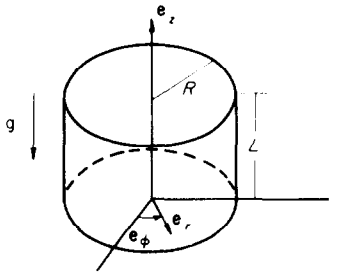

FIG. 1. Schematic of physical system.

the gravitational field is directed in the negative z-direction. The vertical temperature profile is initially linear with temperature T_1 on the upper boundary and T_0 on the lower boundary, where $T_0 > T_1$. The thermal conductivity (k), heat capacity (C_p) and viscosity (μ) are assumed constant. The fluid density (ρ) is assumed to be a linear function of temperature: $\rho = \rho_0(1 - \alpha(T - T_0))$. The effect of the temperature dependence of ρ is assumed negligible except in the gravitational body force term appearing in the linear momentum equation (that is, the usual Boussinesq approximation [25] is made). Applying the above assumptions and neglecting second order terms, the conservation equations of mass, linear momentum and energy lead to the following set of linear nondimensional equations for determining the amplitude of the perturbation of velocity (U), temperature (Θ) and pressure (P):

$$\nabla \cdot \mathbf{U} = 0 \tag{1}$$

$$Pr^{-1}\frac{\partial \mathbf{U}}{\partial t} + \nabla P - \nabla^2 \mathbf{U} - Ra^{\frac{1}{2}}\Theta \mathbf{e}_z = 0, \tag{2}$$

$$\frac{\partial \Theta}{\partial t} - \nabla^2 \Theta - Ra^{\frac{1}{2}}(\mathbf{e}_z \cdot \mathbf{U}) = 0, \tag{3}$$

where

$$\mathbf{U} = U_r\mathbf{e}_r + U_\varphi \mathbf{e}_\varphi + U_z\mathbf{e}_z,$$

$$\nabla \cdot \mathbf{U} = (r\gamma)^{-1}\frac{\partial}{\partial r}(rU_r) + (r\gamma)^{-1}\frac{\partial U_\varphi}{\partial \varphi} + \frac{\partial U_z}{\partial z},$$

$$\nabla P = \gamma^{-1}\frac{\partial P}{\partial r}\mathbf{e}_r + (r\gamma)^{-1}\frac{\partial P}{\partial \varphi}\mathbf{e}_\varphi + \frac{\partial P}{\partial z},$$

$$\nabla^2\Theta = r^{-1}\gamma^{-2}\frac{\partial}{\partial r}\left(r\frac{\partial \Theta}{\partial r}\right) + (r\gamma)^{-2}\frac{\partial^2\Theta}{\partial \varphi^2} + \frac{\partial^2\Theta}{\partial z^2},$$

$$\nabla^2\mathbf{U} = \left\{\gamma^{-2}\frac{\partial}{\partial r}\left[r^{-1}\frac{\partial}{\partial r}(rU_r)\right] + (r\gamma)^{-2}\frac{\partial^2 Ur}{\partial \varphi^2} - 2(r\gamma)^{-2}\frac{\partial U_\varphi}{\partial \varphi} + \frac{\partial^2 U_r}{\partial z^2}\right\}\mathbf{e}_r$$

$$+\left\{\gamma^{-2}\frac{\partial}{\partial r}\left[r^{-1}\frac{\partial}{\partial r}(rU_\varphi)\right] + (r\gamma)^{-2}\frac{\partial^2 U_\varphi}{\partial \varphi^2} + 2(r\gamma)^{-2}\frac{\partial U_r}{\partial \varphi} + \frac{\partial^2 U_\varphi}{\partial z^2}\right\}\mathbf{e}_\varphi$$

$$+\left\{r^{-1}\gamma^{-2}\frac{\partial}{\partial r}\left(r\frac{\partial U_z}{\partial r}\right) + (r\gamma)^{-2}\frac{\partial^2 U_z}{\partial \varphi^2} + \frac{\partial^2 U_z}{\partial z^2}\right\}\mathbf{e}_z.$$

Note that the particular nondimensionalization used here leads to the appearance of an aspect ratio, γ, in the differential operators but simply fied future integrations since the range of both independent variables r and z is 0 to 1. Axisymmetric solutions of equations (1)–(3) are sought for two sets of boundary conditions.

$$\mathbf{U} = 0;\ \Theta = 0 \qquad r = 1, \qquad 0 \leqslant z \leqslant 1, \tag{4}$$

$$\mathbf{U} = 0;\ \Theta = 0 \qquad z = 0, 1 \qquad 0 \leqslant r \leqslant 1, \tag{5}$$

and

$$\mathbf{U} = 0 \qquad r = 1, \qquad 0 \leqslant z \leqslant 1, \tag{6}$$

$$\mathbf{U} = 0;\ \Theta = 0 \qquad z = 0, 1, \qquad 0 \leqslant r \leqslant 1, \tag{7}$$

$$\frac{\partial \Theta}{\partial r} = 0 \qquad r = 1, \qquad 0 \leqslant z \leqslant 1. \tag{8}$$

The first corresponds to conducting walls on the top, bottom, and side, and the second corresponds to conducting walls on the top and bottom, and insulating side boundary.

It is physically obvious and easily established by direct substitution that the system (1)–(8) is invarient to the following transformation:

$$r \to r, \qquad \varphi \to \varphi, \qquad z \to z + 0{\cdot}5 \tag{9}$$

That is, the system is invariant to a translation of the coordinate origin to the middle of the layer. After having performed the translation, the system is also invariant with respect to the following transformation:

1. $U_r(r, \varphi, z) \to -U_r(r, \varphi, -z)$,
   $U_\varphi(r, \varphi, z) \to -U_\varphi(r, \varphi, -z)$,
   $U_z(r, \varphi, z) \to U_z(r. \varphi, -z)$,
   $\Theta(r, \varphi, z) \to \Theta(r, \varphi, -z)$,
   $P(r, \varphi, z) \to -P(r, \varphi, -z)$;

2. $U_r(r, \varphi, z) \to U_r(r, \varphi, -z)$,
   $U_\varphi(r, \varphi, z) \to U_\varphi(r, \varphi, -z)$
   $U_z(r, \varphi, z) \to -U_z(r, \varphi, -z)$,
   $\Theta(r, \varphi, z) \to -\Theta(r, \varphi, -z)$,
   $P(r, \varphi, z) \to P(r, \varphi, -z)$.

Consequently, for example the functions U_z and Θ (or U_r, U_φ and P) generated in the solution of system (1)–(8) separate into two two classes, i.e. an even and odd class about $z = 0{\cdot}5$. The importance of these symmetry properties lies in the insight which they provide in the choice of appropriate trial functions for the Rayleigh–Ritz technique described in Section 4.

Because of the linearity and invariance of the system (1)–(8) with respect to a translation of zero time, solutions of the following form are sought:

$$\mathbf{U}: \mathbf{u}(r, z)\, e^{\sigma t}, \tag{10}$$

$$\Theta: \theta(r, z)\, e^{\sigma t}, \tag{11}$$

$$P: p(r, z)\, e^{\sigma t}, \tag{12}$$

In general, u, θ and p are complex-valued functions. Substituting the representation (10)–(12) into equations (1)–(3) leads to:

$$\nabla \cdot \mathbf{u} = 0, \tag{13}$$

$$Pr^{-1}\sigma \mathbf{u} + \nabla p - \nabla^2 \mathbf{u} - Ra^{\frac{1}{2}}\theta \mathbf{e}_z = 0, \tag{14}$$

$$\sigma\theta - \nabla^2\theta - Ra^{\frac{1}{2}}(\mathbf{e}_z \cdot \mathbf{u}) = 0. \tag{15}$$

Finally, it is more convenient to recast system (13)–(15) in matrix form by defining

$$\mathbf{L} = \begin{bmatrix} (Pr^{-1}\sigma - \nabla^2) & -Ra^{\frac{1}{2}}\mathbf{e}_z \\ -Ra^{\frac{1}{2}}\mathbf{e}_z & (\sigma - \nabla^2) \end{bmatrix}$$

$$\boldsymbol{\varphi} = \begin{bmatrix} \mathbf{u} \\ \theta \end{bmatrix}.$$

Then system (13)–(15) becomes

$$\mathbf{L}\boldsymbol{\varphi} + \begin{bmatrix} \nabla P \\ 0 \end{bmatrix} = \begin{bmatrix} 0 \\ 0 \end{bmatrix} \tag{16}$$

plus the restriction that the velocity field $\mathbf{u}$ associated with $\boldsymbol{\varphi}$ be solenoidal, i.e. $\nabla \cdot \mathbf{u} = 0$.

3. VARIATIONAL FORMULATION

In order to recast the stability problem in a variational form, certain symmetry properties of the mathematical description are utilized. In examining the symmetry, it is convenient to define the inner product of two vector-valued functions as

$$\langle \mathbf{a}, \mathbf{b} \rangle = \int_V \tilde{\mathbf{b}} \cdot \mathbf{a}\, dv$$

Then

$$\langle \boldsymbol{\varphi}^*, \mathbf{L}\boldsymbol{\varphi} \rangle = \int_V [Pr^{-1}\sigma(\mathbf{u}^* \cdot \mathbf{u}) + \nabla \mathbf{u}^* : (\nabla \mathbf{u})^\dagger - Ra^{\frac{1}{2}}\theta(\mathbf{e}_z \cdot \mathbf{u}^*) - Ra^{\frac{1}{2}}\theta^*(\mathbf{e}_z \cdot u) + \sigma\theta^*\theta + \nabla\theta^* \cdot \nabla\theta]\, dv + \int_{\partial V} \mathbf{n} \cdot (\mathbf{u}^* \cdot (\nabla u)^\dagger)\, da + \int_{\partial V} \theta^* \mathbf{n} \cdot \nabla\theta\, da \tag{17}$$

follows directly from (13)–(15) and Green's theorem. A second application of Green's theorem and the restriction that $\mathbf{u}^*$ and θ^*

assume boundary conditions identical to those assumed by $\mathbf{u}$ and θ simplifies (17) to

$$\langle \boldsymbol{\varphi}^*, \mathbf{L}\boldsymbol{\varphi} \rangle = \langle \boldsymbol{\varphi}, \mathbf{L}\boldsymbol{\varphi}^* \rangle.$$

Consequently the adjoint of the operator $\mathbf{L}$ relative to the inner product $\langle , \rangle$, denoted $\mathbf{L}^*$, is $\mathbf{L}$, i.e. $\mathbf{L} = \mathbf{L}^*$, meaning $\mathbf{L}$ is a formally self-adjoint operator. Moreover, since in deriving $\mathbf{L}^*$, it is restricted that $\boldsymbol{\varphi}^*$ be equal to $\boldsymbol{\varphi}$ on the boundary ∂V, the domain of the operator $\mathbf{L}^*$ equals the domain of $\mathbf{L}$. Therefore, the differential system $\mathbf{L}$ plus boundary data represents a self-adjoint system. The self-adjointness of the governing equations with respect to either set of boundary conditions guarantees that the marginal stability state ($\sigma_r = 0$) for both cases is characterized by $\sigma_i = 0$, that is, the so-called principle of exchange of stabilities is valid [26] and an oscillatory instability cannot occur. It is noteworthy that in this case $\mathbf{u}$, θ and p can be assumed to be real valued functions without loss of generality.

The mathematical characterization of the marginal stability state is:

$$\nabla \cdot \mathbf{u} = 0, \tag{18}$$

$$\nabla^2 \mathbf{u} + Ra^{\frac{1}{2}}\theta \mathbf{e}_z - \nabla p = 0, \tag{19}$$

$$\nabla^2 \theta + Ra^{\frac{1}{2}}(\mathbf{e}_z \cdot \mathbf{u}) = 0, \tag{20}$$

coupled with the appropriate boundary conditions (4)–(5) or (6)–(8). As mentioned earlier this system of equations plus the appropriate boundary conditions is non-separable, that is, a planform function cannot be introduced as in the infinite layer case which is detailed in Chandrasekhar [6]. Consequently, here, an approximate solution is obtained by recasting the equations in variational form and using approximate methods of solution.

It has been shown [26] that the solution of the variational problem

$$\lambda = \underset{(\mathbf{u},\theta)\varepsilon\,\mathscr{V}}{\text{maximum}} \frac{2\int_V \theta(\mathbf{e}_z \cdot \mathbf{u})\,dv}{\int_V [\nabla \mathbf{u} : (\nabla \mathbf{u})^\dagger + \nabla\theta \cdot \nabla\theta]\,dv},$$

$$\lambda \equiv Ra^{-\frac{1}{2}} \tag{21}$$

is the solution of the system (18)–(20) if $\mathscr{V}$ is a linear vector space of couples $(\mathbf{u}, \theta)$, i.e. a vector field and an associated scalar field, each containing a solenoidal velocity vector field, and each satsifying the constraints $\mathbf{u} = \mathbf{0}$ on ∂V and either $\theta = 0$ on ∂V corresponding to conditions (4)–(5) or $\theta = 0$ at $z = 0,1, 0 \leqslant r \leqslant 1$, corresponding to (6)–(8). It is noteworthy that in the case of boundary conditions (6)–(8) the conditions $\partial/\partial r = 0$ at $r = 1$, $0 \leqslant z \leqslant 1$, does not have to be satisfied by couples in $\mathscr{V}$ since it is a so-called natural, or unstable, boundary condition and will automatically be satisfied by the temperature field θ associated with the maximizing couple. (See Mikhlin [27] for a detailed treatment of natural boundary conditions.)

4. RAYLEIGH–RITZ APPROXIMATION AND TRIAL FUNCTIONS

The Rayleigh–Ritz technique is used to generate an upper bound approximation to the critical Rayleigh number (*here, "critical" refers to the lowest Rayleigh number at which a stationary axisymmetric pattern of motion can prevail mathematically*) as well as an approximation to the corresponding dynamic state of the system. As is well-known [27], the Rayleigh–Ritz approximation method reduces the extremal problem to a finite dimensional problem by restricting the linear vector space $\mathscr{V}$ appearing in (21) to a subspace $\mathscr{V}' \subseteq \mathscr{V}$. The latter restriction is implemented by representing the approximate solution in terms of a linear combination of linearly independent couples $(\mathbf{u}_i, \theta_i)$ which are contained in $\mathscr{V}'$ and form a basis in $\mathscr{V}'$. Therefore, if λ' is the approximation to λ which is generated in $\mathscr{V}'$, it follows directly that $\lambda' \leqslant \lambda$, and in general $\lambda' \leqslant \lambda'' \leqslant \ldots \leqslant \lambda$, if $\mathscr{V}' \subseteq \mathscr{V}'' \subseteq \ldots \subseteq \mathscr{V}$. That is, as the number of possible couples in competition increases, the maximum can never decrease. In terms of the critical Rayleigh number, it follows that the Rayleigh–Ritz technique leads to an upper bound.

In applying the Rayleigh–Ritz method, it is convenient to use the following representations

for $\mathbf{u}$ and θ in (21):

$$\mathbf{u} = \sum_{i=1}^{N}\sum_{j=1}^{M} B_{ij}\left[\frac{1}{r}X_j'(z)\,Y_i(r)\,\mathbf{e}_r - \frac{1}{r}X_j(z)\,Y_1(r)\,\mathbf{e}_z\right] \tag{22}$$

$$\theta = \sum_{i=1}^{N}\sum_{j=1}^{M} A_{ij}\,J_0(\alpha_i r)\sin(j\pi z). \tag{23}$$

Here a prime denotes differentiation with respect to the argument. The corresponding approximate Stokes streamfunction is

$$\psi = \sum_{i=1}^{N}\sum_{j=1}^{M} B_{ij}\,Y_i(r)\,X_j(z). \tag{24}$$

The functions $Y_i(r)$ and $X_j(z)$ are eigenfunctions of the following eigenvalue problems:

$$\left(\frac{\mathrm{d}^2}{\mathrm{d}r^2} + \frac{1}{r}\frac{\mathrm{d}}{\mathrm{d}r} - \frac{1}{r^2}\right)^2 [r^{-1}\,Y_i(r)] \equiv \left[r\frac{\mathrm{d}}{\mathrm{d}r}\left(\frac{1}{r}\frac{\mathrm{d}}{\mathrm{d}r}\right)\right]^2 Y_i(r) = \xi_i^4 Y_i(r), \tag{25}$$

$$Y_i(r) = Y_i'(r) = 0 \qquad r = 1, \tag{26}$$

$$Y_i(r),\ Y_i'(r) \text{ finite} \qquad r = 0, \tag{27}$$

and

$$\frac{\mathrm{d}^4}{\mathrm{d}z^4}X_j(z) = \delta_j^4 X_j(z) \tag{28}$$

$$X_j(z) = X_j'(z) = 0 \qquad z = 0, 1. \tag{29}$$

Finally, the α's are roots of either

$$J_0(\alpha_k) = 0 \qquad \text{(conducting sides)}, \tag{30}$$

or

$$J_1(\alpha_k) = 0 \qquad \text{(insulating sides)}. \tag{31}$$

These conditions insure that the trial solution satisfies the linear independence property and boundary conditions appropriate to the Rayleigh–Ritz method. Also the axial trial functions, X_j's, fall into two classes, respectively even and odd functions about $z = 0{\cdot}5$, and hence the symmetry properties satisfied by the exact solution are satisfied by this choice of trial functions. Here the insulating side conditions $\mathrm{d}\theta/\mathrm{d}r = 0$, $r = 1$, is satisfied even though it is a natural boundary condition. It is hoped that this will result in a better representation of the temperature and velocity fields.

Substituting the representations (22) and (23) into (21) leads to the finite dimensional extremal problem of maximizing the functional

$$I = 2\int_V \theta(\mathbf{e}_z\cdot\mathbf{u})\,\mathrm{d}v - \lambda'\int_V (\nabla\mathbf{u}:(\nabla\mathbf{u}) + \nabla\theta\cdot\nabla\theta)\,\mathrm{d}v, \tag{32}$$

which is now only a function of the $2NM$ variables A_{ij}, B_{ij}. The necessary conditions for a maximum are

$$\frac{\partial I}{\partial A_{ij}} = 0 \qquad i = 1, 2, \ldots, N;\quad j = 1, 2, \ldots, M, \tag{33}$$

$$\frac{\partial I}{\partial B_{ij}} = 0 \qquad i = 1, 2, \ldots, N;\quad j = 1, 2, \ldots, M. \tag{34}$$

These conditions lead to the following system of linear, homogeneous algebraic equations (i.e. an algebraic eigenvalue problem) for determining $\lambda \equiv Ra^{-\frac{1}{4}}$ and the constants A_{ij} and B_{ij} up to a multiplicative constant for M either odd (corresponding to the even mode in z) or even (corresponding to the odd mode in z):

$$\sum_{n,m}\left\{2B_{mn}\left[\int_0^1 Y_m'(r)\,J_0(\alpha_i r)\,\mathrm{d}r\right]\cdot\left[\int_0^1 X_n(z)\sin(j\pi z)\,\mathrm{d}z\right]\right\} + \lambda\left\{A_{ij}\gamma^2(JJ/2)\left[\left(\frac{\alpha_i}{\gamma}\right)^2 + (j\pi)^2\right]\right\} = 0, \tag{35}$$

$$\sum_{n,m}\left\{A_{mn}\left[\int_0^1 Y_i'(r)\,J_0(\alpha_m r)\,dr\right]\right.$$

$$\left.+\left[\int_0^1 X_j(z)\sin(n\pi z)\,dz\right]\right\}$$

$$+\lambda\left[\left[B_{ij}\left[\delta_j^4+\left(\frac{\xi_i}{\gamma}\right)^4\right][J_1^2(\xi_i)]\right.\right.$$

$$+\frac{2}{\gamma^2}\sum_{k,q}\left\{B_{kq}\left[\int_0^1 r^{-1}Y_q'(r)Y_k'(r)\,dr\right]\right.$$

$$\left.\left.\left.\times\left[\int_0^1 X_j'(z)\,X_q'(z)\,dz\right]\right\}\right]=0, \qquad (36)$$

where $m, k = 1, 2, \ldots, N$;

$n, q = 1, 3, \ldots, M$ if M is an odd integer;
$n, q = 2, 4, \ldots, M$ if M is an even integer;
$JJ = J_1^2(\alpha_i)$ for conducting sides;
$JJ = J_0^2(\alpha_i)$ for insulating sides.

To facilitate the solution of this set of algebraic equations, generated by the Rayleigh–Ritz technique, the equations are recast in the form of a matrix eigenvalue problem in terms of the B-coefficients. The resulting matrix eigenvalue problem yields an upper bound to the critical Rayleigh number and the corresponding sets of approximate velocity coefficients (B_{ij}'s). The associated set of temperature coefficients are obtained by solving the matrix equation relating the A_{ij}'s and B_{ij}'s. The streamfunction corresponding to a calculated eigenvalue was calculated by substituting the velocity coefficients into equation (24), and then the number of radial rolls was determined from the streamlines as displayed in Figs. 2–6. Note that the streamlines are displayed only for z values between 0·5 and 1·0 since they are symmetric about $z = 0{\cdot}5$.

5. LOWER BOUND TO CRITICAL RAYLEIGH NUMBER

A lower bound to the critical Rayleigh number can be generated by reconsidering the basic variational formulation. Suppose the ratio of the quadratic forms appearing in (21) is maximized with respect to couples $(\mathbf{u}, \theta)$ contained in a linear vector space $\mathscr{V}^*$ which includes $\mathscr{V}$, i.e. $\mathscr{V} \subseteq \mathscr{V}^*$. It is obvious that the maximum cannot decrease and hence if λ^* is the maximum value of (21) in $\mathscr{V}^*$, it follows

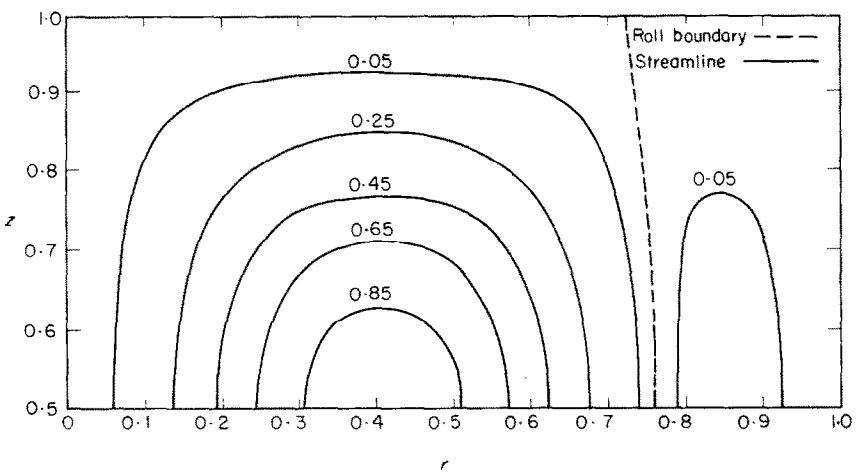

FIG. 2. Streamlines for conducting lateral walls at the critical Rayleigh number and $\gamma = 1{\cdot}70$.

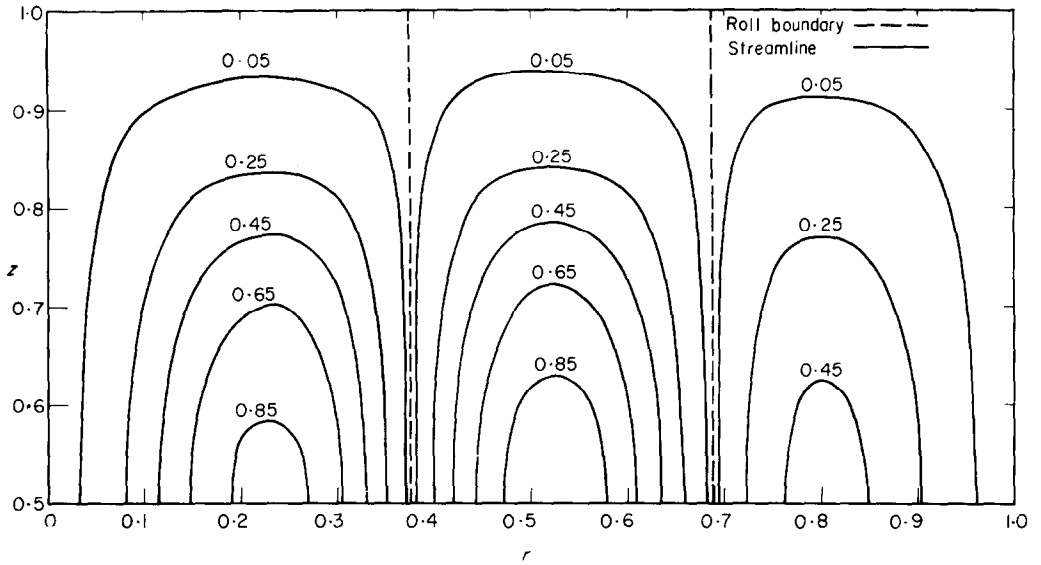

FIG. 3. Streamlines for conducting lateral walls at the critical Rayleigh number and $\gamma = 3.25$.

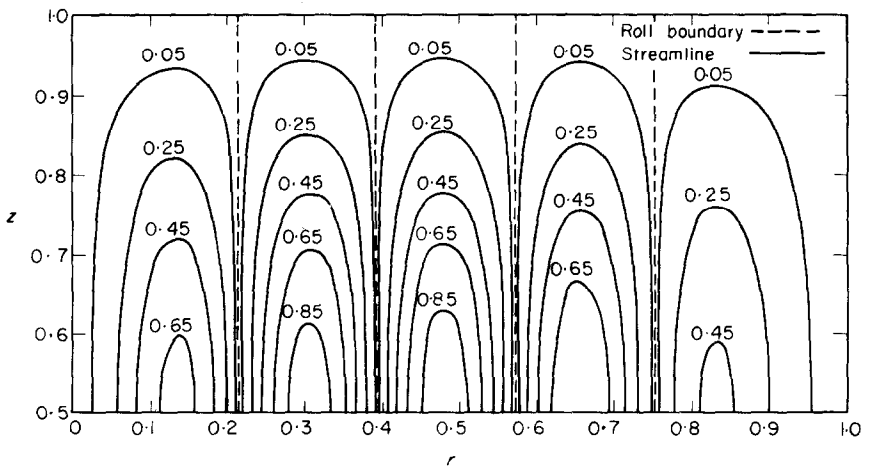

FIG. 4. Streamlines for conducting lateral walls at the critical Rayleigh number and $\gamma = 5.75$.

that $\lambda \leqslant \lambda^*$ or $Ra^* \leqslant Ra_{\text{critical}}$. Thus a lower bound to Ra_{critical} is generated.

To implement this scheme computationally, a suitable linear vector space $\mathscr{V}^*$ must be be devised. Here one such computationally convenient choice is to impose the same smoothness requirements of couples as in $\mathscr{V}$ but not to require the temperature and tangential component of the velocity field to vanish at the lateral boundaries of the cylinder. The Euler equations appropriate to the variational problem (31) over $\mathscr{V}^*$ instead of $\mathscr{V}$ lead to the differential equations (18)–(20) but with the new boundary conditions:

$$\mathbf{u} = \mathbf{0}; \quad \theta = 0 \qquad z = 0,1, \quad 0 \leqslant r \leqslant 1; \tag{37}$$

$$\left.\begin{aligned} &\mathbf{e}_r \cdot \mathbf{u} = 0 \\ &\mathbf{e}_r \cdot \nabla u_z = 0 \\ &\mathbf{e}_r \cdot \nabla \theta = 0 \end{aligned}\right\} \qquad r = 1, \quad 0 \leqslant z \leqslant 1; \tag{38}$$

where $u_z \equiv \mathbf{e}_z \cdot \mathbf{u}$. This mathematical problem corresponds to allowing "slip" at the lateral walls in the physical system. An exact solution to (18)–(20), (37) and (38) can be obtained after Pellew and Southwell [20] and Zierep [8] by the method of separation of variables. This method leads to a Stokes streamfunction of the form

$$\psi = CrJ_1(ar)\,F(z) \tag{39}$$

where $F(z)$ satisfies a differential eigenvalue problem identical to the one obtained by Pellew and Southwell [20] for the case of an infinite fluid layer. The permissible values of a, the so-called wave number, are, for fixed values

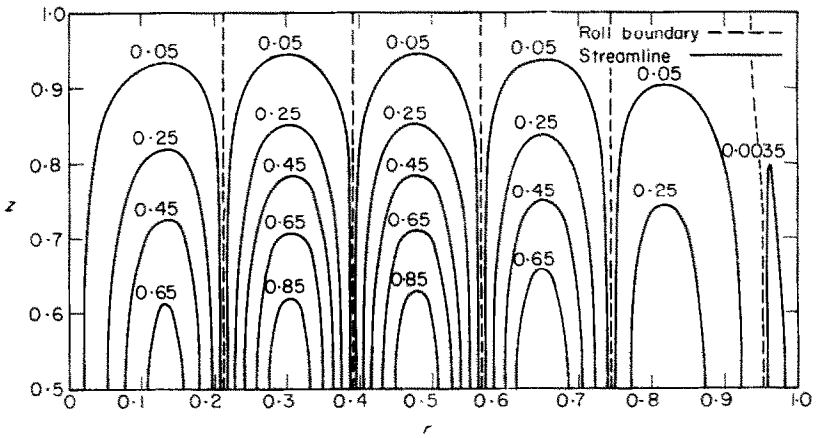

FIG. 5. Streamlines for insulating lateral walls at the critical Rayleigh number and $\gamma = 5{\cdot}75$.

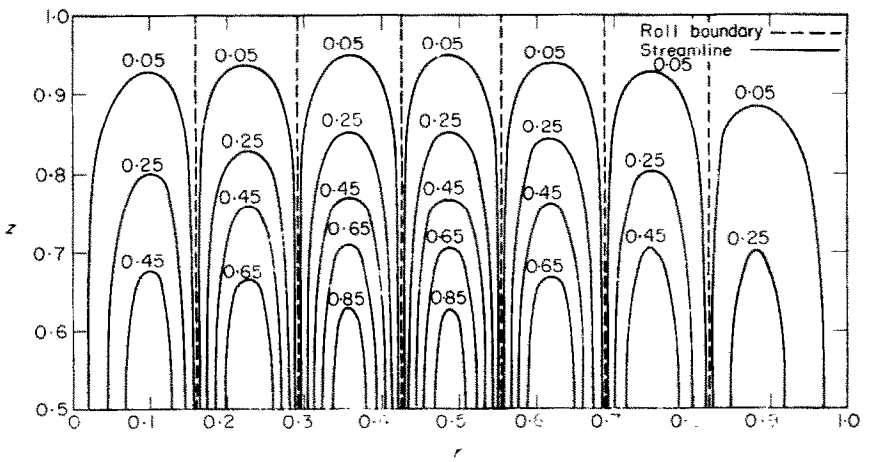

FIG. 6. Streamlines for insulating lateral walls at the critical Rayleigh number and $\gamma = 7{\cdot}75$.

of the aspect ratio γ, the roots of the transcendental equation: $J_1(a\gamma) = 0$. Once the permissible value of a are obtained, the corresponding Rayleigh numbers are computed by solving the eigenvalue problem associated with $F(z)$ and the permissible values of a. If the roots of $J_1(a\gamma) = 0$ are denoted by η_k, then the permissible values of a are $a_k = \eta_k \gamma^{-1}$. It is apparent from an inspection of (39) that the kth root η_k and corresponding wave number a_k are associated with a flow which has k radial rolls. The corresponding locus of lower bound Rayleigh numbers is indicated by the ——– —— line in Fig. 7; also indicated is the number of radial rolls. It is noteworthy that the number of rolls increases with aspect ratio, and also that if the number of radial rolls is fixed there is always an aspect ratio which yields the smallest value of the Rayleigh number, i.e. 1708.

6. DISCUSSION AND RESULTS

In forming the system of algebraic equations to be solved for the approximate Rayleigh numbers and associated sets of temperature and velocity coefficients (A_{ij} and B_{ij}), it was noted that two noncombining forms of the solution, respectively even and odd about $z = 0{\cdot}5$, result.

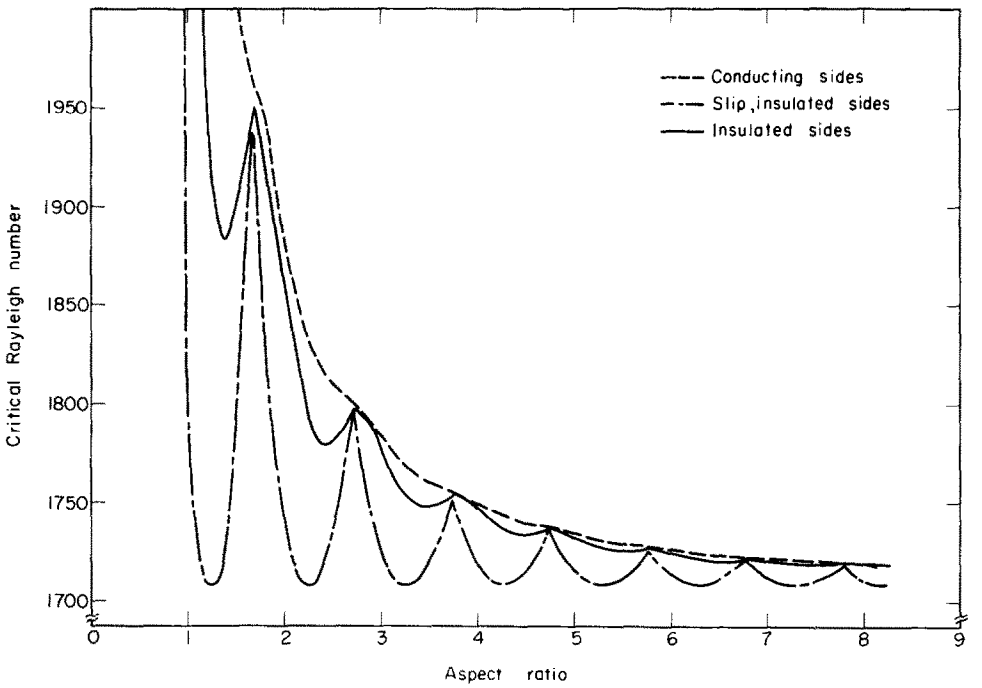

FIG. 7. Overall stability curves for bounded cylindrical layer.

For an aspect ratio equal to, or greater than, 0·5, the even solution in z, corresponding to an odd number of vertical rolls, is the most unstable. At an aspect ratio of 0·5, for example, the Rayleigh number appropriate to the first even mode for conducting side walls is 11 725 whereas the Rayleigh number for the first odd mode is 31 122. This comparison is typical of those obtained at larger aspect ratios and henceforth, for aspect ratios greater than 0·5 only even solutions [corresponding to $j = 1, 3, 5, \ldots$ in $X_j(z)$ and $\sin(j\pi z)$] are considered. Consequently

Table 1. Conducting sides. The three smallest Rayleigh numbers (Ra_1, Ra_2, Ra_3) *and the number of radial rolls predicted are tabulated for aspect ratios from 0·5 to 8·0*

Aspect ratio	Ra_1	Rolls	Ra_2	Rolls	Ra_3	Rolls
0·50	11725·08	1	71006·91	--	95107·44	--
1·00	2545·02	1	7334·75	--	20698·84	--
1·25	2124·87	1	4266·56	2	10237·14	3
1·50	2009·61	1	3089·59	--	6179·77	--
1·60	1988·77	2	2849·38	2	5276·88	3
1·70	1968·00	2	2689·77	2	4605·75	3
1·75	1956·11	2	2633·12	2	4336·82	3
2·00	1886·24	2	2472·73	--	4336·82	--
2·25	1833·35	2	2323·95	3	3113·50	2
2·50	1810·31	2	2159·90	--	2898·34	--
2·58	1806·60	2	2118·32	3	2814·87	--
2·66	1803·32	3	2084·08	3	2727·68	4
2·665	1803·12	3	2082·19	3	2722·23	4
2·67	1802·91	3	2080·32	3	2716·79	4
2·68	1802·49	3	2076·68	3	2705·94	4
2·69	1802·06	3	2073·15	3	2695·13	4
2·71	1801·18	3	2066·44	3	2673·69	4
2·74	1799·79	3	2057·19	3	2642·05	4
2·75	1799·30	3	2054·32	3	2631·68	4
2·83	1794·97	3	2034·92	--	2552·55	--
3·00	1783·55	3	2008·99	--	2413·76	--
3·083	1777·79	3	1999·49	4	2362·70	4
3·25	1767·89	3	1976·75	4	2292·77	2
3·416	1761·60	3	1946·30	4	2253·66	3
3·50	1759·62	3	1929·99	--	2237·03	--
3·75	1755·56	4	1890·51	4	2170·50	5
4·00	1749·68	4	1871·08	--	2091·08	--
4·25	1743·01	4	1858·86	5	2036·05	5
4·50	1739·11	4	1839·80	--	2010·37	--
4·75	1737·17	5	1821·05	5	1985·19	6
5·00	1734·36	5	1810·98	--	1948·99	--
5·25	1730·95	5	1804·98	6	1919·89	6
5·50	1728·87	5	1796·36	--	1905·75	--
5·75	1727·82	6	1785·10	6	1893·42	7
6·00	1726·25	6	1779·41	--	1873·99	--
6·25	1724·29	6	1776·06	7	1857·12	5
6·50	1723·10	6	1770·42	--	1849·03	--
6·75	1722·50	7	1764·25	7	1842·12	6
7·00	1721·49	7	1760·98	--	1830·35	--
7·25	1720·24	7	1759·06	8	1820·23	6
7·50	1719·55	7	1755·41	--	1816·09	--
7·75	1719·20	7	1751·62	8	1811·91	9
8·00	1718·53	8	1750·03	--	1804·25	--

-- signifies number of rolls not determined for given Rayleigh number.

the instability is manifested as a single vertical roll and varying number of radial rolls.

Rayleigh numbers and the corresponding sets of velocity and temperature coefficients were obtained with $N = 10$ and $M = 5$, i.e. for ten radial trial functions and 3 ($M = 1, 3, 5$) vertical trial functions. This choice of trial solution allows the approximation of dynamic states with up to 10 radial rolls and 1, 3 or 5 vertical rolls, and yields Rayleigh numbers in the aspect

Table 2. Insulating sides. The three smallest Rayleigh numbers (Ra_1, Ra_2, Ra_3) *and the number of radial rolls predicted are tabulated for aspect ratios from* 0·5 *to* 8·0

Aspect ratio	Ra_1	Rolls	Ra_2	Rolls	Ra_3	Rolls
0·50	10887·15	1	68048·09	2	86729·72	3
1·0	2261·86	1	6631·50	2	19265·47	3
1·25	1920·83	1	3777·60	2	9351·86	3
1·50	1896·13	1	2677·94	2	5548·23	3
1·60	1921·99	1	2448·78	2	4701·15	3
1·70	1946·48	2	2303·90	2	4067·04	3
1·75	1949·86	2	2264·26	2	3810·07	3
2·00	1862·27	2	2329·06	2	2940·43	3
2·25	1791·92	2	2315·21	3	2727·49	1
2·50	1780·81	2	2082·78	3	2889·57	2
2·60	1786·43	2	2016·39	3	2778·51	4
2·665	1790·93	2	1983·16	3	2680·44	4
2·70	1793·07	2	1968·73	3	2628·55	4
2·75	1795·17	3	1952·62	3	2557·80	4
2·80	1795·50	3	1942·14	3	2491·80	4
2·90	1789·73	3	1937·65	3	2374·89	4
3·00	1778·25	3	1949·40	3	2278·11	4
3·25	1752·99	3	1976·04	4	2143·97	2
3·50	1747·24	3	1908·06	4	2189·69	2
3·75	1752·90	3	1849·44	4	2163·46	5
4·00	1747·95	4	1841·51	4	2042·71	5
4·25	1736·39	4	1856·28	5	1967·74	5
4·50	1732·93	4	1832·41	5	1975·39	3
4·75	1734·54	4	1801·39	5	1985·32	6
5·00	1733·78	5	1794·33	5	1930·12	6
5·25	1727·67	5	1802·22	6	1884·69	6
5·50	1725·30	5	1792·95	6	1881·67	4
5·75	1726·57	5	1774·95	6	1892·48	5
6·00	1725·98	6	1769·02	6	1867·55	7
6·25	1722·48	6	1773·30	6	1838·22	7
6·50	1720·72	6	1770·05	7	1831·62	5
6·75	1721·35	6	1759·06	7	1839·25	6
7·00	1721·36	7	1753·89	7	1829·30	8
7·25	1719·33	7	1756·02	7	1809·79	8
7·50	1717·95	7	1755·59	7	1801·99	6
7·75	1718·17	7	1748·91	8	1806·96	6
8·00	1718·39	8	1744·45	8	1805·57	9

ratio range considered here accurate to the fourth significant figure based on the change in Rayleigh number when 5 additional radial trial functions ($N = 15$) or 1 additional axial trial function ($M = 7$) are added. The three smallest Rayleigh numbers and the corresponding number of radial rolls determined from streamlines are tabulated in Tables 1 and 2 for conducting and insulating lateral walls, respectively.

The stability curves for insulating and conducting side walls are presented in Fig. 7. The corresponding number of radial rolls can can be obtained from Tables 1 and 2. The stability curve for insulated lateral boundaries has peaks at the aspect ratios at which the number of rolls predicted increases, similar to the lower bound case where an independent stability curve existed for a given number of rolls. This characteristic is not evident in the stability

curve for conducting sides although inflection points seem to occur at these transition points. In both curves the number of rolls increases with increasing aspect ratio. This increase in the number of rolls in both cases, is characterized by the gradual growth of the roll nearest the wall, followed by the formation of the additional roll from this larger roll as is illustrated in Fig. 8. In this figure the radial velocity component is displayed as a function of radius at $z = 0{\cdot}25$ (or $z = 0{\cdot}75$ since the solution is symmetric about $z = 0{\cdot}5$) at aspect ratios near the transition point from 2 to 3 rolls for insulated lateral boundaries.

The range of aspect ratios over which a given number of rolls is predicted seems nearly uniform in both cases after the appearance of the second roll, being approximately a unit of aspect ratio in width. The transition in the number of rolls occurs, for both insulating and conducting lateral walls, near aspect ratio values of 2·75, 3·75, 4·75, . . . for a transition from 2, 3, 4, . . . radial rolls to 3, 4, 5, . . . rolls, respectively. This compares with the wavelength relation

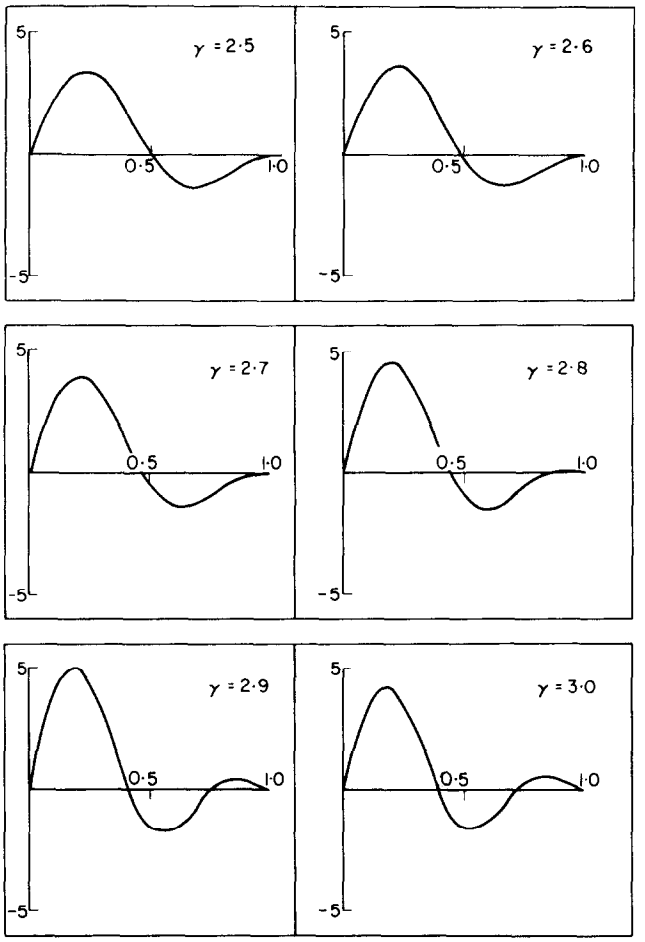

FIG. 8. Radial component of velocity for insulating lateral walls.

Table 3

Aspect ratio	Ra_1	Rolls	Ra_2	Rolls	Ra_3	Rolls
A. Conducting sides						
9·852	1714·66	10	1733·89	10	1768·27	9
10·30	1713·94	10	1732·26	11	1761·68	11
12·987	1711·86	13	1723·08	13	1742·61	14
B. Insulating sides						
9·852	1714·44	10	1731·38	10	1767·94	9
10·30	1713·49	10	1731·57	10	1756·96	11
12·987	1711·69	13	1721·76	13	1742·32	14

ship for the infinite layer case [23]:

$$n\lambda = \frac{R}{L}. \tag{40}$$

λ, the wavelength, is the ratio of the width of one roll (one roll corresponds to one half of a roll cell in the infinite layer terminology) to the fluid layer depth; n is the number of rolls; and R/L is the aspect ratio. From linear theory for an infinite layer, λ, as defined here, has a value of 1·008 at the critical Rayleigh number [6]. Therefore, (40) would suggest that the number of rolls would roughly correspond to the aspect ratio, a fact that the results mentioned above bear out.

In order to present an overall stability picture for a cylindrical layer of fluid, the upper bound stability curves for insulating and conducting lateral walls, and the lower bound stability curve of insulating slip walls are displayed in Fig. 7. The important feature here is that the distance between the lower bound and the upper bound is at worst only about 20 per cent of the average critical Rayleigh number predicted and this distance rapidly decreases as the aspect ratio increases. The convergence of the upper and

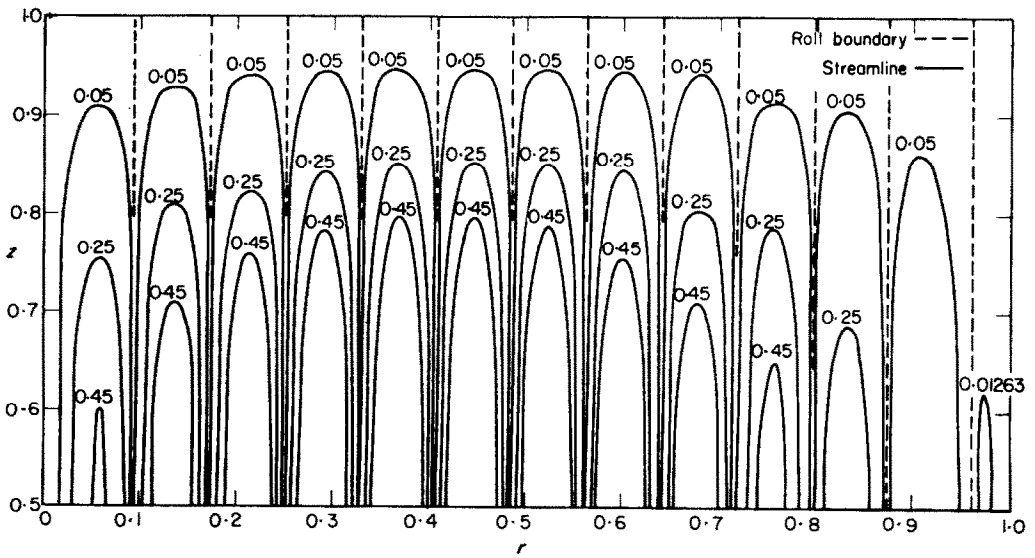

FIG. 9. Streamlines for insulating walls at the critical Rayleigh numbers and $\gamma = 12{\cdot}987$.

lower bounds stability curves at large aspect ratios is indicative of the lessening influence of the lateral boundary on the stability of the system. Also noteworthy is the fact that the upper and lower bound stability curves converge very near to one another at those aspect ratios near which the number of rolls predicted changes.

The relative order of the stability curves for insulating and conducting lateral boundaries is derivable from the variational formulation and is a manifestation of the less constrained temperature field associated with the insulating case. As was pointed out in Section 3, the elements of the linear vector space $\mathscr{V}$ associated with the variational formulation (21) are not required to satisfy the condition $\mathbf{e}_r \cdot \nabla\theta = 0, r = 1, 0 \leqslant z \leqslant 1$ appropriate to an insulating lateral boundary because this condition is a natural boundary condition. Consequently the space $\mathscr{V}$ associated with the insulating side wall problem includes the space associated with the conducting side wall problem as a subspace. Therefore, the maximum of (21) for the insulating side wall case cannot be smaller than the corresponding maximum for the conducting case, or

$$Ra_{\text{insulating}} \leqslant Ra_{\text{conducting}}.$$

The fact that the approximate critical Rayleigh number for insulating side walls lies below that for conducting side walls affords a good check on the accuracy of the matrix eigenvalue routine used here, especially when applied at large aspect ratios.

Koschmieder's experimental observations, [13], [22] and [23], were made at aspect ratios of 9·852, 10·30 and 12·987, and a résumé of the appropriate analytical predictions, using 19 radial trial functions and 3 axial trial functions, is presented in Table 3 and an example of the corresponding streamlines is displayed in Fig. 9. In Table 1, Ra_1 is the critical Rayleigh number, and Ra_2 and Ra_3 are the Rayleigh numbers corresponding to the second and third eigenvalues, respectively.

At both 9·852 and 10·30, the approximate analysis for either insulating or conducting sides predicts 10 radial rolls at the critical Rayleigh number, agreeing with Koschmieder's observations. At 9·852, Koschmieder observed that the number of rolls decreases to 9 at a super-critical value of the Rayleigh number [13]; at 10·30 he observed an increase to 11 rolls [22]. Both of these trends are suggested by the number of radial rolls associated with the second and third eigenvalues if one invisions a supercritical instability of the first state and a stable supercritical flow associated with the second, or third, state. This possibility is suggested since it has been shown [28] that each of the simple eigenvalues (Rayleigh numbers) of the linear stability problem corresponds to a bifurcation point of the nonlinear stability problem. That is, there exist steady, finite amplitude, axisymmetric flows at Rayleigh numbers arbitrarily close to the Rayleigh number stability limits predicted by linear theory. The results can be displayed qualitatively as in Fig. 10 where A

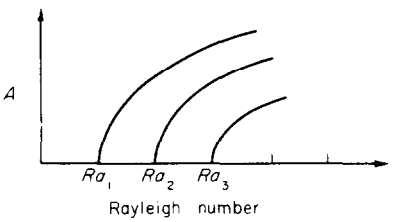

FIG. 10. Qualitative sketch of nonlinear stability results.

represents some characteristic amplitude of the flow. ($A = 0$ for $Ra < Ra_1$ since it has been shown [29] that subcritical instabilities cannot occur.) Steady, finite amplitude, axisymmetric flows are possible along the solid lines in Fig. 10. Moreover, at each bifurcation point (intersection of solid line with line $A = 0$) the structure of the finite amplitude flow is "close" to the flow associated with the appropriate solution of the linear stability problem. That is, the number of vertical cells and radial rolls should be identical in the limit of zero flow amplitude. If one assumes that the structure of the flow at the bifurcation points persists to larger values of the

Rayleigh number, i.e. along the solid lines in Fig. 10, then, for example, when $Ra_2 < Ra < Ra_3$ steady flows with the number of radial rolls associated with the Ra_1- or Ra_2-solution of the linear stability problem would be possible. The one which is observed would then depend on the stability of these flows.

At an aspect ratio of 12·987, the approximate analysis predicts thirteen rolls for either conducting or insulating lateral walls, again agreeing with Koschmieder's observation near the critical Rayleigh number [23]. The number of rolls associated with the second and third eigenvalues, together with the results at 9·852 and 10·30 serve to point out the fact that in the present case no general pattern of monotonic increase or decrease in the number of radial rolls can be associated with the succeeding higher order Rayleigh numbers (eigenvalues) predicted using approximate linear stability analysis.

ACKNOWLEDGEMENTS

The authors wish to thank Dr. G. Homsy for many helpful discussions and assistance in some of the initial computations and Professor A. Acrivos for his valuable suggestions.

REFERENCES

1. H. Bénard, Les tourbillons cellulaire dans une nappe liquide, *Revue Gen. Sci. Pur. Appl.* **11**, 1261–1271 (1900).
2. H. Bénard, Les tourbillons cellulaires dans une nappe liquide transportant de la chaleur par convection en régime permanent, *Annls Chim. Phys.* **23**, 62–144 (1901).
3. M. J. Block, Surface tension as the cause of Bénard cells and surface deformation in a liquid film, *Nature, Lond.* **178**, 650–651 (1956).
4. J. R. A. Pearson, On convection cells induced by surface tension, *J. Fluid Mech.* **4**, 489–500 (1958).
5. Lord Rayleigh, On convective currents in a horizontal layer of fluid when the higher temperature is on the under side, *Phil. Mag.* **32**, 529–546 (1916).
6. S. Chandrasekhar, *Hydrodynamic and Hydromagnetic Stability*. Clarendon Press, Oxford (1961).
7. S. Ostrach and D. Pneuli, The thermal instability of completely confined fluids inside some particular configurations, *J. Heat Transfer* **85**, 1346–1354 (1963).
8. J. Zierep, Zur theorie der zellularkonvektion V., *Beitr. Phys. Atmos.* **36**, 70–76 (1963).
9. S. H. Davis, Convection in a box: linear theory, *J. Fluid Mech.* **30**, 465–478 (1967).
10. S. H. Davis, Convection in a box: on the dependence of preferred wave-number upon the Rayleigh number at finite amplitude, *J. Fluid Mech.* **32**, 619–624 (1968).
11. S. F. Liang, A. Vidal and A. Acrivos, Buoyancy-driven convection in cylindrical geometries, *J. Fluid Mech.* **36**, 239–256 (1969).
12. D. K. Edwards, Suppression of cellular convection by lateral walls, *J. Heat Transfer* **91**, 145–150 (1969).
13. E. Koschmieder, On convection on a uniformly heated plane, *Beitr. Phys. Atmos.* **39**, 1–11 (1966).
14. M. M. Chen and J. A. Whitehead, Evolution of two-dimensional periodic Rayleigh convection cells of arbitrary wave-numbers, *J. Fluid Mech.* **31**, 1–15 (1968).
15. A. C. Newell and J. A. Whitehead, Finite bandwidth, finite amplitude convection, *J. Fluid Mech.* **38**, 279–303 (1969).
16. L. A. Segel, Distant side-walls cause slow amplitude modulation of cellular convection, *J. Fluid Mech.* **38**, 293–224 (1969).
17. L. A. Segel and J. T. Stuart, On the question of the preferred mode in cellular thermal convection, *J. Fluid Mech.* **13**, 289–306 (1962).
18. A. Schluter, D. Lortz and F. Busse, On the stability of steady finite amplitude convection, *J. Fluid Mech.* **23**, 129–144 (1965).
19. S. H. Davis and L. A. Segel, Effects of surface curvature and property variation on cellular convection, *Physics Fluids* **11**, 479–476 (1968).
20. A. Pellew and R. V. Southwell, On maintained convective motion in a fluid heated from below, *Proc. R. Soc.* **176A**. 312–343 (1940).
21. M. Sherman and S. Ostrach, Lower bounds to the critical Rayleigh number in completely confined regions, *J. Appl. Mech.* **34**, 308–312 (1967).
22. E. Koschmieder, On convection on a uniformly heated rotating plane, *Beitr. Phys. Atmos.* **40**, 216–225 (1967).
23. E. Koschmieder, On the wavelength of convective motions, *J. Fluid Mech.* **35**, 527–530 (1969).
24. R. Soberman, Effects of lateral boundaries on natural convection, *J. Appl. Phys.* **29**, 872–873 (1958).
25. J. Boussinesq, *Théorie Analytique de la Chaleur*, 161, **2**, p. 172. Gauther-Villars, Paris (1903).
26. R. L. Sani, Convective instability, Ph.D. Thesis, University of Minnesota, Minneapolis (1963).
27. S. Mikhlin, *Variational Methods of Mathematical Physics*. Pergamon Press, Oxford (1964).
28. R. L. Sani, Free convective instability, *Mathematica Jap.* **12**, 81–99 (1967).
29. R. L. Sani, On the non-existence of subcritical instabilities in fluid layers heated from below, *J. Fluid Mech.* **20**, 315–319 (1964).

INSTABILITÉ THERMOCONVECTIVE DANS UNE COUCHE FLUIDE CYLINDRIQUE LIMITÉE

Résumé—Le début de la convection avec symétrie de révolution dans des couches cylindriques de fluides chauffées par en-dessous est étudié pour différents rapports du rayon à la hauteur. On a calculé les bornes supérieures et inférieures du nombre de Rayleigh critique, et examiné la structure de l'écoulement de convection. Cette dernière est en bon accord avec les observations de Koschmieder.

THERMISCHE INSTABILITÄT IN BEGRENZTEN FLÜSSIGKEITSSCHICHTEN

Zusammenfassung—Das Einsetzen von achsensymmetrischer Konvektion in zylindrischen Flüssigkeitsschichten, die von unten beheizt werden, ist für zahlreiche Radius-Höhe-Verhältnisse untersucht worden. Es wurde die obere und untere Grenze der kritischen Rayleighzahl für derartige Strömungen berechnet und die Struktur der Konvektionserhöhung untersucht. Die Ergebnisse dieser Untersuchung stehen in guter Übereinstimmung mit den Beobachtungen von Koschmieder.

ТЕРМОКОНВЕКТИВНАЯ НЕУСТОЙЧИВОСТЬ В ОГРАНИЧЕННОМ ЦИЛИНДРИЧЕСКОМ СЛОЕ ЖИДКОСТИ

Аннотация—Исследуется возникновение осесимметричной конвекции в цилиндрических слоях жидкости, нагреваемой снизу, для различных отношений радиуса к высоте. Рассчитываются верхние и нижние границы критического числа Релея для таких течений и изучается структура конвективного потока. Последнее находится в хорошем соответствии с наблюдениями Кошмидера.